Journal of Materials Chemistry C

Accepted Manuscript

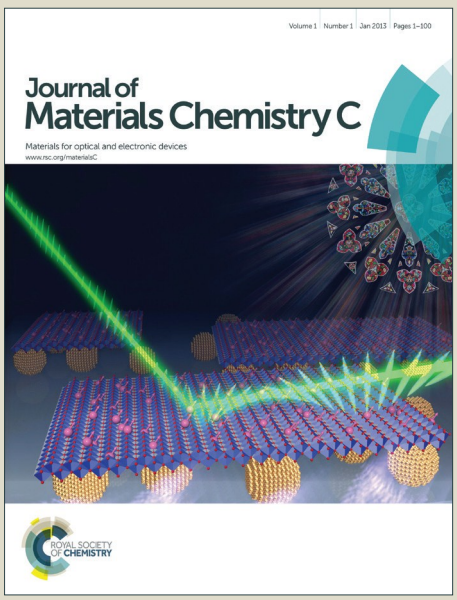

ROYAL SOCIETY OF CHEMISTRY

www.rsc.org/materialsC

Structural, Magnetic and Dielectric Properties of Two Novel Mixed-Valence Iron(II)-Iron(III) Metal Formate Frameworks

Mirosław Mączka,*[,a] Aneta Ciupa,[a] Anna Gągor,[a] Adam Sieradzki,[b] Adam Pikul,[a] and Maciej Ptak[a]

[a]*Institute of Low Temperature and Structure Research, Polish Academy of Sciences, Box 1410, 50-950 Wrocław 2, Poland*

[b]*Department of Experimental Physics, Wrocław University of Technology, Wybrzeże Wyspiańskiego 27, 50-370, Wrocław, Poland*

ABSTRACT

Two novel mixed-valence iron(II)-iron(III) formate frameworks templated by ethylammonium and diethylammonium cations have been prepared and characterized by DSC, x-ray diffraction and spectroscopic methods. We also report dielectric and magnetic properties of the obtained samples. Both MOFs crystallize in the $P\bar{3}1c$ structure and exhibit magnetic order at 39 K. The analogue with diethylammonium cation undergoes a structural phase transition near 240 K into a triclinic phase. This transition has an order-disorder character and it is associated with pronounced dielectric anomaly. This compound is therefore the second discovered mixed-valence metal formate exhibiting multiferroic properties.

Introduction

A lot of attention has been focused in recent years on the design of materials with various functionalities. In this respect, metal-organic frameworks (MOFs) have emerged as a particularly promising group of compounds for technological applications since almost infinite number of organic ligands and metal combinations provide a possibility of tuning the structural, magnetic, electric, catalytic, luminescence and many other properties.[1] Among various ligands, formate anion has attracted much interest because of its ability to bridge two metal ions and mediating magnetic interactions between them.[2] Extensive studies of divalent metal formates templated by NH_4^+ or protonated amines with general formula [cat][$M(HCOO)_3$] (M=Cd, Mg, Zn, Mn, Fe, Co, Ni, Cu) showed that they crystallize in the perovskite or chiral structures and many of them undergo order-disorder phase transitions.[3-7] Among these compounds, coexistence of magnetic and ferroelectric order was proved for dimethylammonium (DMA) and ammonium analogues by observation of good dielectric hysteresis loops and pyroelectric current as well as magnetic order at 8-36 K.[3-5,8] Another interesting property of these compounds is negative linear compressibility discovered for [NH_4][$Zn(HCOO)_3$].[9] Some of these compounds also exhibit giant dielectric constants, ferroelastic properties and rich polymorphism under compression.[9-13] It has also been shown very recently that it is possible to dope some of these materials at sites occupied by alkylammonium cations (by other alkylammonium cation) or divalent metal cations (by trivalent cations) and such doping changes character of the phase transition into diffused one.[14,15]

Apart of widely studied divalent metal formates, a few heterometallic and one mixed-valence formates were also synthesized and characterized. One family of such compounds crystallizes in the perovskite structure and up to now only two compounds belonging to this group are known,

i.e., $[(CH_3)_2NH_2][Na_{0.5}Fe_{0.5}(HCOO)_3]$ and $[(CH_3)_2NH_2][Na_{0.5}Cr_{0.5}(HCOO)_3]$.[16,17] Another group has the general formula $[(CH_3)_2NH_2][M^{II}Fe^{III}(HCOO)_6]$ (M^{II}=Fe, Co, Mn, Mg, Ni, Zn, Cu).[18-22] The first member of this family, i.e., intensely colored mixed-valence formate $[(CH_3)_2NH_2][Fe^{II}Fe^{III}(HCOO)_6]$, **1**, was synthesized in 2009 by Hagen *et al.*[18] Later, heterometallic analogues with Fe^{III} and divalent cations other than Fe^{II} were also obtained and characterized.[19,21,22] Except for Cu analogue (*C2/c* space group),[22] **1** and all heterometallic compounds crystallize in the trigonal space group ($P\bar{3}1c$).[18-22] **1** and analogues with Mn, Co, Ni and Cu exhibit magnetic ordering at 28.5-42 K.[19,22] It is worth adding that only the mixed-valence compound **1** undergoes an order-disorder phase transition into an antiferroelectric $R\bar{3}c$ phase around 152-155 K, i.e., only this compound exhibits multiferroic properties.[20,21]

Herein, we report synthesis of two novel mixed-valence metal formates, i.e. $[C_2H_5NH_3][Fe^{II}Fe^{III}(HCOO)_6]$, **2**, and $[(C_2H_5)_2NH_2][Fe^{II}Fe^{III}(HCOO)_6]$, **3**. We will show that use of bulkier ethylammonium (EtA) and diethylammonium (DEtA) cations has significant effect on properties of these mixed-valence MOFs.

Experimental

Synthesis

All reagents (analytically grade) used for synthesis are commercially available and used without further purification. Elemental analysis (C, H, N) was performed on a Elementar Vario EL CHNS analyzer. Compound **2** was synthesized by heating a mixture containing 35 ml of N-ethylformamide, 25 ml HCOOH, 1.5 mmol $FeCl_2$ and 1.5 mmol $FeCl_3$ in a Teflon-lined microwave autoclave at 140°C for 24 h. Black crystals obtained after overnight cooling were washed by ethanol and dried at room temperature. Compound **3** was prepared by the same

procedure using N,N-diethylformamide. A good match of their powder XRD patterns confirmed the phase purity of both bulk samples with a simulation from the single-crystal structural data (Figure S1 in the Supporting Information). Anal. Calcd for **2** (%): C, 22.44; H, 3.27; N, 3.27; Found (%): C, 22.41; H, 3.26; N, 3.14. Anal. Calcd for **3** (%): C, 26.33; H, 3.95; N, 3.07; Found (%): C, 26.29; H, 3.86; N, 3.13.

Heat Capacity

Heat capacity was measured using Mettler Toledo DSC-1 calorimeter with high resolution of 0.4 μW. Sample weight was chosen to be 12.61 mg. Sample was slightly crushed to ensure good thermal contact. Nitrogen was used as a purging gas. Temperature change rate was chosen to be 5 K/min and the DSC thermograms were taken for both cooling and heating cycles. The excess heat capacity associated with the phase transition was calculated by subtraction from the data the baseline representing variation in the absence of the phase transitions.

Dielectric Properties

The temperature-dependent dielectric measurements were carried out using the experimental set-up made by Novo-Control Alpha GmbH. This system was equipped with a Novocontrol Alpha dielectric spectrometer, having a frequency range of 10^{-1} to 10^{6} Hz. Since the obtained single crystals were not big enough to perform single crystal dielectric measurements, pellets made of well-dried samples were measured instead. The pellets were placed between two copper, flat electrodes (diameter 6mm) of the capacitor with a gap of 0.3 mm. Temperature was controlled using the nitrogen gas cryostat, with the stability higher than 0.1 K. Temperature was changed within the range from 150 to 275 K, with a step of 1 K. The small signal of an amplitude 1V was applied across the sample.

Magnetic Properties

Magnetic properties of a large number of freely oriented small single crystals were measured using a commercial superconducting quantum interference device (SQUID) magnetometer in the temperature range 2−60 K and in external magnetic fields up to 50 kOe in the following way. First, the samples were cooled down in zero magnetic field from room temperature down to 2 K, at which the magnetization was measured as a function of magnetic field increasing up to 50 kOe and decreasing down to 0 Oe. Subsequently the magnetic field of 100 Oe was set up and the magnetization was measured as a function of temperature increasing up to 60 K and decreasing down to 2 K. The background coming from the weakly diamagnetic sample holder (not shown here) was found to be negligible; thus its subtraction was omitted. Also no demagnetization corrections were made to the data reported here.

Crystal Structure Determination

Single-crystal x-ray diffraction experiment was carried out on the Xcalibur Atlas diffractometer equipped with Mo *K*α radiation and CCD detector. Intensities were measured in ω-scan mode with $\Delta\omega=1.0^{o}$ using CrysAlis CCD program. Empirical absorption correction with spherical harmonics was done using multi-scan CrysAlis PRO (Agilent Technologies, Version 1.171.37.35h). The structure refinement was performed by means of *SHELXL2014*/7.[23] Due to the disorder of counterions the nitrogen and carbon atoms were refined isotopically. Hydrogen atoms were included in geometric positions (C-H~0.96 Å, N-H~0.89 Å) and treated as riding atoms. The $U_{iso}(H)$ values were constrained to be $1.2U_{eq}$ (carrier atom). Also the C-N distance restrains were used to obtain reasonable geometry of counterions.

Powder XRD pattern was obtained for all samples on an X'Pert PRO X-ray diffraction system equipped with a PIXcel ultrafast line detector, focusing mirror, and Soller slits for $CuK\alpha_1$ radiation (λ=1.54056 Å). The low-temperature XRD pattern of **3** was recorded in transmission mode using the capillary of 0.3mm in diameter. The low temperature was maintained by open-flow nitrogen gas system (Oxford Cryosystem). The powder data were processed using Jana2006.[24] The details of the crystal data and structure refinement are given in Table S1. Selected bonds and angles are presented in Table 1.

IR studies

Temperature-dependent IR spectra were measured for the samples in KBr pellets in the range of 3800-400 cm^{-1} with the Biorad 575C FT-IR spectrometer using a helium-flow Oxford cryostat. The spectral resolution was 2 cm^{-1}.

Results and discussion

Thermal Properties

DSC data show that **2** does not undergo any phase transition upon cooling to 130 K but **3** exhibits a strong thermal anomaly around 242 K upon warming and 237 upon cooling (Figure S2). The change in heat capacity and entropy related to the phase transition is presented in Figure 1. The calculated change in enthalpy ΔH and entropy ΔS is about 1.62 $KJmol^{-1}$ and 7.2 $Jmol^{-1}K^{-1}$, respectively. Since according to the X-ray diffraction data the $DEtA^+$ cation occupies three disordered sites in the room temperature phase (N=3, see discussion in the next paragraph of the present paper), a complete ordering of these cations should lead to $\Delta S = Rln(N) = 9.1$ $Jmol^{-1}K^{-1}$.

The observed ΔS value is close to that expected, indicating 3-fold order-disorder character of the phase transition.

Figure 1. Heat capacity of **3** measured in heating mode. The insets show the change in C_p and S related to the phase transition.

Structural Studies

2 and **3** possess a niccolite-type metal anionic $[Fe^{II}Fe^{III}(HCOO)_6]^-$ framework with template cations located in the cavities expanding along the *c* axis. The crystal structure is isomorphic to reported previously $[(CH_3)_2NH_2][M^{II}Fe^{III}(HCOO)_6]$ metal formates with M^{II}=Fe, Co, Mn.[18,19] The crystal system is trigonal with $P\bar{3}1c$ space group (Tables S1). The metal centers are linked by the formate ions in the *anti-anti* configuration. Both have trigonally distorted octahedral oxygen coordination. The Fe-O distances equal to 2.129(2)/2.122(3)Å for Fe^{II} on 3.2 symmetry site and 2.004(2)/2.008(2)Å for Fe^{III} on -3.. site in **3**/**2** which implies ordering of iron Fe^{III} and Fe^{II} ions in the $[Fe^{II}Fe^{III}(HCOO)_6]^-$ framework (see Figure 2a and Table 1). Statistical distribution of Fe^{III} and M^{II} ions, manifesting in a uniform Fe^{III}/M^{II}-O distances for both metal centers, has been observed so far for $[(CH_3)_2NH_2][M^{II}Fe^{III}(HCOO)_6]$ where M^{II} was Mg, Ni.[21,22] The crystal cavities in the

niccolite structure form channels expanding along the *c* axis which may accommodate even large counterions such as $DEtA^+$. The template cations are disordered in the $P\bar{3}1c$ phase over three equivalent positions with a site occupation factor equal to 1/3 for each setting; see Figures 2a and 2b. $DEtA^+$ may perform free rotations along the *c* axis changing the possible sites. It is involved in two symmetrical N-H···O hydrogen bonds with the metal-formate framework, with donor to acceptor distance of 3.217(8) Å and donor-to acceptor angle of 173(1)° (Figure 2c). EtA^+ ions are disordered over six possible positions (Figure 2d). Interestingly, this much smaller template induces noteworthy elongation of the framework in the *c* axis compared to $DEtA^+$; 14.1221(5) *vs*. 13.7058(4) Å. However, simultaneous contraction in the *a* and *b* directions ultimately results in a smaller volume of the unit cell; 828.26(5) $Å^3$ in **2** vs. 847.18(5) $Å^3$ in **3**. In both compounds the disorder is a consequence of the steric effect (the presence of large cavities) and the symmetry of the templates, which is lower than the symmetry of the crystal (inducing splitting of the atomic positions).

Figure 2. (a) The crystal structure of **3**. The crystal cavities are filled with disordered $DEtA^+$ template. The Fe^{III} and Fe^{II} ions are ordered. (b) Each $DEtA^+$ cation may occupy three different positions with site occupation factor of 1/3. (c) One of the three allowed $DEtA^+$ orientations in the niccolite cavity. The N-H···O hydrogen bonds between the template and the framework are marked as dashed lines. (d) One of the six possible orientations of the EtA^+ in **2**.

Table 1. Selected geometric parameters for **2** and **3** (Å, º).

	3	**2**

$Fe(1)^{II}$—O1 x 6	2.129(2)	2.122(3)
$Fe(2)^{III}$—$O2^{i}$ x 6	2.004(2)	2.008(2)
O(1)—C	1.227(3)	1.232(5)
O(2)—C	1.249(3)	1.248(5)
O—$Fe(1)^{2+}$—O_{cis}	86.0(1)- 93.45(8)	85.9(2)-92.8(1)
O—$Fe(1)^{2+}$—O_{trans}	179.2(1)	178.2(2)
O—$Fe(2)^{3+}$—O_{cis}	88.84(8)- 91.16(8)	88.79(1)-91.2(1)
O—$Fe(2)^{3+}$—O_{trans}	180.0(1)	180.0(1)
C—O(1)—Fe(1)	126.9(2)	126.4(3)
C—O(2)—Fe(2)	129.72(18)	127.5(3)
O(1)—C—O(2)	125.8(3)	1244(4)

Symmetry code(s): (i) *-x+y, -x, z*;

Below 242 K, **3** undergoes the structural phase transition. The distortion of the crystal structure leads to the symmetry decrease from the trigonal to the triclinic. The phase transition is of the translationengleiche type, *i.e.* the order of the point group is reduced without changing of the translations.[25] Consequently, the resultant unit cell in the triclinic phase is the distorted high temperature cell with only small volume changes from 847.2(1) $Å^3$ at 260 K to 838.2(1) $Å^3$ in 205 K. The contraction of the unit cell volume with temperature lowering may be associated with ordering of the template. Because the transition from $P\bar{3}1c$ to $P1$ or $P\bar{1}$ subgroup is of index 6, six structural twin domains are expected to appear with symmetry lowering. And indeed the reconstructions of the reciprocal space taken in the triclinic phase reveal splitting of the diffraction patterns from one (in the trigonal phase) into six after the symmetry reduction. Figure S3 illustrates the splitting of the diffraction patterns as well as the Le Bail fit of the powder data

using the triclinic unit cell with parameters a=8.307(1)Å, b=8.585(1)Å, c=13.540(1)Å, α=89.5(1)°, β=89.3(1)°, γ=119.7(1)°.

Magnetic Properties

Figures 3a and 3b present results of magnetic properties measurements performed for **2** and **3** using the same measurement sequence described above. As seen, in both compounds a sharp anomaly in temperature dependence of the magnetization is visible at T_{ord} of about 39 K, manifesting ordering of the magnetic moments of Fe^{III} and Fe^{II} ions. Slightly lower T_{ord} of about 37 K was reported for **1**.[19] Below T_{ord} the magnetization measured upon warming up changes in a different way than upon cooling down. In particular, as far as the temperature increases, the magnetization (marked as M_{up}) decreases and vanishes at a compensation temperature T_{comp} of 26 K (in **2**) and 22 K (in **3**). Upon further warming up M_{up} still decreases and changes its sign to negative. Afterwards it goes through a shallow minimum and increases back towards zero. Very similar behavior was also reported for **1** with T_{comp} of 29 K.[19] Above the ordering temperature the magnetization of **2** and **3** is weakly positive (hardly noticeable due to the scale used in Figure 3), as expected for a paramagnetic state. In turn, the shapes of the $M_{down}(T)$ curves look like mirror reflections of $M_{up}(T)$'s. In particular, upon cooling down the magnetization of both samples jumps again below the T_{ord}, yet it remains positive down to T_{comp} and becomes negative below this temperature. At the lowest temperature both M_{up} and M_{down} evolve towards a Brillouin-like shape (positive or negative) and saturate at similar absolute values (of about 4 emu/g in **2** or 2 emu/g in **3**), which suggests full reversal of the total magnetization in the systems studied upon changing magnetic history of the sample. Field dependence of M shows in both compounds weak magnetic

hysteresis (stronger in **2**), which corroborates the ferro- or ferrimagnetic character of the phase transitions at T_{ord}.

The temperature-induced reversal of the magnetization M_{down} below T_{comp} is predicted by Néel's classic theory for N-type ferrimagnets. Their ground state is determined by an interplay of two antiparallel ferromagnetic sublattices with different saturation magnetization and different temperature dependences.[26-28] As a result, one can observe a compensation point (T_{comp}) at which the net magnetization of the two sublattices cancel each other. Below T_{comp} the negative spontaneous magnetization of one of the sublattices is thermodynamically favored over the postitive one of the other sublattice, which leads to total negative magnetization at low temperatures. The observed full reversal of the magnetization just after applying 50 kOe (see the M_{up} curve in Figure 3) shows that the magnetocrystalline anisotropy in the compounds studied is weaker than the field applied. As discussed by Zhao *et al*., the very large negative magnetization in molecular-based magnets is very rare,[19] but it was recently discovered in similar formate framework templated by DMA^+ cations.[19,20]

It is worth adding that other heterometallic niccolites of general formula $[(CH_3)_2NH_2][M^{II}Fe^{III}(HCOO)_6]$ (M^{II}=Co, Mn, Ni, Cu) showed typical positive magnetization at low temperatures and shape of the observed magnetic anomalies indicated that these compounds exhibit weak ferrimagnetism.[19,22] The temperature at which the long-range magnetic order occurs was the highest for M^{II}=Ni (42 K) and it decreased to 35, 32 and 28.5 K for the Mn, Co and Cu formate, respectively.[19,22] Very recently, magnetic studies were also reported for $[(CH_3)_2NH_2][M^{II}Cr^{III}(HCOO)_6]$ (M^{II}= Ni, Cu) niccolites.[29] These studies showed that magnetic properties of the chromium and iron compounds are very similar each to other but the ordering temperatures of the chromium compounds were about twice lower than the isostructural iron-based compounds.[29]

Weak ferrimagnetism was also reported for niccolites of the general formula [amineH_2^{2+}] [$M^{II}_2(HCOO)_6$] with amine= N,N'-dimethylethylenediamine and 1,4-diaminobutane ($NH_2(CH_2)_4NH_2$), M^{II}=Mn, Fe, Co, Ni.[30,31] The magnetic ordering temperatures of N,N'-dimethylethylenediammonium metal formates were reported as 33.7, 19.8, 16.4 and 8.6 K for Ni, Fe, Co and Mn, respectively.[30] As can be noticed, they are significantly lower (by about 8-17 K) compared to the iron-based heterometallic niccolites. This comparison shows that presence of Fe^{III} in the metal formate framework leads to strengthening of the magnetic interactions.

Figure 3. Temperature variation of magnetization *M* of (a) **2** and (b) **3** measured in increasing and decreasing temperature in a constant magnetic field *H*; the arrows mark the ordering (T_{ord}) and

compenstation (T_{comp}) temperatures. Inset: field dependence of M measured at constant temperature T upon increasing and decreasing H (open and closed symbols, respectively).

Optical properties

The both samples show a very broad inter-valence charge transfer (IVCT) band near 600 nm (Figure S4). These bands are very similar to that observed for **1**,[16] indicating that all these compounds are type II mixed-valence compounds.

Dielectric Studies

In order to determine if the phase transition in **3** is associated with some dielectric anomaly, real part of the dielectric permittivity was measured as a function of temperature (Figure 4). The real part of the dielectric permittivity takes relatively high values (around 30) when compared to those of previously reported perovskite analogues.[7,16] Similar value was, however, reported for $[NH_3(CH_2)_4NH_3][Co_2(HCOO)_6]$ niccolite.[31] High values were also reported for niccolite-type $[NH_3(CH_2)_4NH_3][Mg_2(HCOO)_6]$ (near 70 at 1 MHz) and **1** (about 60).[32,20] The temperature dependence of the relative permittivity bears some resemblance to that observed for **1,** where the phase transition from paraelectric to antiferroelectric occurs.[20] That is, for high frequencies (>0.1MHz), the dielectric permittivity exhibits significant monotonic decrease below about 243 K. This dielectric anomaly indicates the occurrence of a phase transition of dipolar character. As the frequency decreases (<100kHz), the dielectric anomaly becomes more obscure in such a way that the real part of dielectric permittivity starts to deviate from the preceding monotonic behavior, and increase more rapidly at temperatures above 245K. Such behavior suggests that

some conductivity process starts to dominate. In such case of conducting sample, the effective analysis of dielectric relaxation requires the use of electric modulus representation $M^* = 1 / \varepsilon^*$.[33] The real and imaginary part of electric modulus versus frequency is shown in Figure S5. The multi-peak shaped spectra with non-Debye relaxation revealed the complexity of dielectric relaxation processes in this sample. Apart from that, however, this results unequivocally confirm the occurrence of ionic conductivity. Increase of the dielectric permittivity at low frequencies and higher temperatures, which can be attributed to ionic conductivity, was observed for many metal formate frameworks,[6,7,31] and it can be most likely attributed to the presence of some amount of water absorbed by the studied pellets.

Figure 4 shows that the dielectric permittivity does not exhibit any strong dielectric dispersion. This behavior is different from that reported for other niccolite-type metal formate frameworks templated by protonated 1,4-diaminobutane, which showed very pronounced frequency dispersions in their dielectric responses.[31,32] This behavior was attributed to the damped motions of the ammonium cation.[31] It is worth noting that strong dielectric dispersion was also observed for perovskites containing dimethylammonium and formamidinium cations in the cavities of the frameworks, i.e., for homometallic formates $[(CH_3)_2NH_2][M^{II}(HCOO)_3]$ (M^{II}=Mg, Ni, Mn) and formamidinium manganese formate as well as heterometallic $[(CH_3)_2NH_2][Na_{0.5}Fe_{0.5}(HCOO)_3]$.[7,16,34]

Figure 4. Temperature dependence of the real part of the dielectric permittivity of **3** at selected frequencies. Dash line corresponds to the structural phase transition temperature.

IR Studies

Additional information on the phase transition mechanism may also be obtained from temperature-dependent IR studies. The recorded IR spectra and temperature dependences of full width at half maximum (FWHM) and wavenumbers for a few selected modes are presented in Figures 5, 6 and S6-S10. The observed wavenumbers and proposed assignments of modes are presented in Table S2.

Let us at first discuss shortly the assignment of modes. Both compounds have similar metal formate frameworks built up of formate, Fe^{II} and Fe^{III} ions. These frameworks are templated either by EtA^+ or $DEtA^+$ cations. Since the lattice modes in formate frameworks are located below 500 cm^{-1}, all IR modes in the 600-3500 cm^{-1} range should be assigned to the internal modes. There are six internal modes of $HCOO^-$ ions: the C-H stretching mode ν_1, the symmetric C-O stretching mode ν_2, the antisymmetric C-O stretching mode ν_4, the symmetric O-C-O

bending (scissor) mode ν_3, the C-H in-plane bending mode ν_5, and the C-H out-of-plane bending mode ν_6.[6,7,35] These modes were observed in narrow wavenumber ranges for different metal formate frameworks.[6,7,35] Assignment of these modes is, therefore, straightforward and will be not discussed here.

Free EtA^+ cation has C_s symmetry and its 27 internal modes are distributed among the irreducible representation: Γ= 16A'+11A".[36] These modes can be subdivided into symmetric stretching ($\nu_s(CH_2)$), antisymmetric stretching (($\nu_{as}(CH_2)$), scissoring ($\delta(CH_2)$), rocking ($\rho(CH_2)$), wagging ($\omega(CH_2)$) and torsion or twisting ($\tau(CH_2)$) modes of the CH_2 group as well as symmetric stretching (ν_s), antisymmetric stretching (ν_{as}), bending (δ), rocking (ρ) and torsion (τ) modes of the CH_3 and NH_3 groups. The remaining three vibrations correspond to symmetric stretching (ν_s(CCN)), antisymmetric stretching (ν_{as}(CCN)) and bending (δ(CCN)) modes of the CCN skeleton. These modes were identified in our spectra based on DFT calculations performed for isolated EtA^+ cation and experimental studies of $[C_2H_5NH_3]_2SiF_6$ and ethylammonium chloride.[36-38]

Free $DEtA^+$ cation has C_{2v} symmetry and 45 internal modes. Similarly to EtA^+, internal modes of $DEtA^+$ can be subdivided into vibrations of CH_3 and CH_2 groups as well as vibrations of skeleton. One may also expect to observe symmetric stretching, antisymmetric stretching, scissoring, rocking, wagging and torsion or twisting modes of the NH_2 group. Studies of vibrational properties of $DEtA^+$ cation are scarce but DFT calculations were published for $[(C_2H_5)_2NH_2]_2SiF_6$.[39] We propose, therefore, assignment of vibrational modes for this cation based on DFT calculations and experimental studies reported for $[(C_2H_5)_2NH_2]_2SiF_6$.[39]

Having discussed assignment of modes, we now move to temperature dependence of IR modes. Figure S6 shows that the spectra of **2** remain qualitatively the same down to 4 K.

Furthermore, temperature dependence of wavenumbers and FWHM values, presented for a few selected modes of **2** in Figures S7 and S8, do not show any anomalies. These data confirm that **2** does not exhibit any structural phase transition. Very weak anomalies appear however between 35 and 40 K, i.e., near the magnetic phase transition temperature. Similar anomalies were reported also for **1** and they can be attributed to spin-phonon coupling.[21]

Temperature-dependent spectra of **3** show different behavior. First of all, many bands exhibit very significant narrowing upon cooling (Figures S9 and 5). This behavior is especially pronounced for the bands corresponding to vibrations of the $DEtA^+$ cation, for instance, $\omega(NH_2)$ and $\rho(NH_2)$ modes (Figure 5 and S10). This behavior proves that ordering of the $DEtA^+$ cations plays a major role in the phase transition mechanism.

Figure 5. Details of the IR spectra of **3** measured at a few selected temperatures. Asterisks show (a) $\omega(NH_2)$ and (b) $\rho(NH_2)$ modes that cannot be clearly observed in the high-temperature phase due to dynamic disorder of $DEtA^+$ cation.

IR data also show that bands corresponding to the ν_{as}(C-C) and ν_{as}(C-N) modes exhibit abrupt shift towards higher wavenumbers upon cooling near T_c (Figure 6). This behavior indicates that the phase transition leads to significant change in the C-N bond lengths and C-N-C bond angles. However, our data do not show splitting of the $DEtA^+$ bands and this result indicates that the low temperature structure contains only one crystallographically distinct $DEtA^+$ cation in the unit cell. Figures 5 and S9 also show that the structural phase transition leads to splitting of majority of bands corresponding to vibrations of the iron formate framework into a few components. This behavior proves that the phase transition is associated with significant distortion of the framework. It is worth noting that weak anomalies are also observed near the magnetic phase transition (see Figure 6 and S10) due to spin-phonon coupling. These anomalies are more pronounced when compared to **2** but comparable to those observed in **1**.[21]

Figure 6. Temperature evolution of a few selected IR wavenumbers of **3** corresponding to (a) $\rho(NH_2)$, (b) ν_{as}(C-C) and ν_{as}(C-N), (c) $\rho(CH_3)$ modes. Vertical lines indicate temperatures of the structural and magnetic phase transitions.

Conclusions

We show that two novel mixed-valence iron(II)-iron(III) formate frameworks templated by EtA^+ and $DEtA^+$ cations can be synthesized using a solvothermal method. It is worth noting that $DEtA^+$ cation has not been yet employed in synthesis of any metal formate framework. We show that size and shape of the alkylammonium cation have significant effect on the lattice parameters, i.e., *c* and *a* changes in the order **2**>**1**>**3** and **3**>**1**>**2**, respectively. The obtained compounds are rare examples of molecular-based magnets with large negative magnetization and **3** is the second discovered mixed-valence metal formate exhibiting multiferroic properties. It is worth noting that contrary to **1**, which shows trigonal $R\bar{3}c$ structure below 152-155 K and a tripling of the unit cell, **3** shows triclinic distortion that occurs at significantly higher temperature (near 240 K) and the phase transition is of the translationengleiche type.

Acknowledgements

This research was supported by the National Science Center (Narodowe Centrum Nauki) in Poland under project No. DEC-2013/11/B/ST5/01058.

Notes

[a]Institute of Low Temperature and Structure Research, Polish Academy of Sciences, Box 1410, 50-950 Wrocław 2, Poland; m.maczka@int.pan.wroc.pl; phone: +48-713954161; fax: +48-713441029

[b]Faculty of Fundamental Problems of Technology, Wrocław University of Technology, Wybrzeże Wyspiańskiego 27, 50-370, Wrocław, Poland

Electronic Supplementary Information (ESI) available: Figures S1-S10: Powder X-ray diffraction, DSC traces, results of the Le Bail fit of the XRD pattern of **3,** diffuse reflectance spectra, IR spectra and temperature dependence of wavenumbers and FWHM of a few selected modes of **2** and **3**. Tables S1 and S2: experimental details for the structure refinement and IR wavenumbers together with proposed assignments.

References

1 R. J. Kuppler, D. J. Timmons, Q. R. Fang, J. R. Li, T. A. Makal, M. D. Young, D. Yuan, D. Zhao, W.; Zhuang, H. C. Zhou, *Coord. Chem. Rev.* 2009, **253,** 3042-3066.

2 Z. Wang, K. Hu, S. Gao and H. Kobayashi, *Adv. Mater.,* 2010, **22,** 1526-1533.

3 P. Jain, V. Ramachandran, R. J. Clark, H. D. Zhou, B. H. Toby, N. S. Dalal and H. W. Kroto, A. K. J. Cheetham, *J. Am. Chem. Soc*., 2009, **131**, 13625-13627.

4 (a) D. W. Fu, W. Zhang, H. L. Cai, Y. Zhang, J. Z. Ge, R. G. Xiong, S. D. Huang and T. Nakamura, *Angew. Chem. Int. Ed*., 2011, **50**, 11947-11951. (b) Y. Tian, J. Cong, S. Shen, Y. Chai, L. Yan, S. Wang and Y. Sun, *Phys. Stat. Sol. RRL* 2014, **8,** 91-94. (c) Y. Tian, A. Stroppa, Y. Chai, L. Yan, S. Wang, P. Barone, S. Picozzi and Y. Sun, *Sci. Rep.* 2014, **4,** 6062.

5 (a) G. C. Xu, W. Zhang, X. M. Ma, Y. H. Hen, L. Zhang, H. L. Cai, Z. M. Wang, R. G. Xiong and S. Gao, *J. Am. Chem. Soc*., 2011, **133**, 14948-14951.

6 M. Maczka, A. Pietraszko, B. Macalik, K. Hermanowicz, *Inorg. Chem*. 2014, **53,** 787-794.

7 (a) M. Mączka, A. Gągor, B. Macalik, A. Pikul, M. Ptak and J. Hanuza, *Inorg. Chem*., 2014, **53**, 457-467. (b) M. Mączka, A. Ciupa, A. Gągor, A. Sieradzki, A. Pikul, B. Macalik and M. Drozd, *Inorg. Chem*., 2014, **53**, 5260-5268.

8 W. Wang, L.-Q. Yan, J.-Z. Cong, Y.-L. Zhao, F. Wang, S.-P. Shen, T. Zhou, D. Zhang, S.-G. Wang, X.-F. Han and Y. Sun, *Sci. Rep*. 2013, **3,** 2024.

9 W. Li, M. R. Probert, M. Kosa, T. D. Bennett, A. Thirumurugan, R. P. Burwood, M. Parinello, J. A. K. Howard, A. K. Cheetham, *J. Am. Chem. Soc.* 2012, **134,** 11940-11943.

10 Y. Imai, B. Zhou, Y. Ito, H. Fijimori, A. Kobayashi, Z. M. Wang, H. Kobayashi, *Chem. Asian J.* 2012, **7,** 2786-2790.

11 W. Li, Z. Zhang, E. G. Bithell, A. S. Batsanov, P. T. Barton, P. J. Saines, P. Jain, C. J. Howard, M. A. Carpeneter, A. K. Cheetham, *Acta Mater*. 2013, **61,** 4928-4938.

12 W. Li, A. Thirumurugan, P. T. Barton, Z. Lin, S. Henke, H. H. M. Yeung, M. T. Wharmby, E. G. Bithell, J. A. K. Howard, A. K.; Cheetham, *J. Am. Chem. Soc.* 2014, **136,** 7801-7804.

13 (a) M. Mączka, P. Kadłubański, P. T. C. Freire, B. Macalik, W. Paraguassu, K. Hermanowicz, J. Hanuza, *Inorg. Chem.* 2014, **53,** 9615-9624. (b) M. Mączka, T. Almeida da Silva, W. Paraguassu and M. Ptak, *Inorg. Chem.* 2014, **53,** 12650-12657.

14 S. Chen, R. Shang, B.-W. Wang, Z.-M. Wang and S. Gao, *Angew. Chem., Int. Ed.;* 2015, **54,** 11093-11096.

15 M. Mączka, A. Sieradzki, B. Bondzior, P. Dereń, J. Hanuza and K. Hermanowicz, *J. Mater. Chem. C*; 2015, **3,** 9337-9345.

16 (a) M. Mączka, A. Pietraszko, L. Macalik, A. Sieradzki, J. Trzmiel and A. Pikul, *Dalton Trans.* 2014, **43,** 17075-17084. (b) A. Sieradzki, J. Trzmiel, M. Ptak and M. Mączka, *Electr. Mater. Lett.* 2015, **11,** 1033-1039.

17 M. Mączka, B. Bondzior, P. Dereń, A. Sieradzki, J. Trzmiel, A. Pietraszko and J. Hanuza, *Dalton Trans.*, 2015, **44,** 6871-6879.

18 K. S. Hagen, S. G. Naik, B. H. Huynh, A. Masello and G. Christou, *J. Am. Chem. Soc*., 2009, **131**, 7516-7517.

19 J.-P. Zhao, B.-W. Hu, F. Lloret, J. Tao, Q. Yang, X.-F. Zhang and X.-H. Bu, *Inorg. Chem*., 2010, **49**, 10390-10399.

20 L. Cañadillas-Delgado, O. Fabelo, J. A. Rodríguez-Velamazán, M.-H. Lemėe-Cailleau, S. A. Mason, E. Pardo, F. Lloret, J.-P. Zhao, X.-H. Bu, V. Simonet, C. V. Colin and J. Rodríguez-Carvajal, *J. Am. Chem. Soc*., 2012, **134**, 19772-19781.

21 A. Ciupa, M. Mączka, A. Gągor, A. Sieradzki, J. Trzmiel, A. Pikul and M. Ptak, *Dalton Trans.*, 2015, **44,** 8846-8854.

22 A. Ciupa, M. Mączka, A. Gągor, A. Pikul and M. Ptak, *Dalton Trans.* 2015, **44,** 13234-13241.

23 G.M. Sheldrick, *Acta Cryst. A,* 2008, **64,** 112-122.

24 V. Petricek, M. Dusek, L. Palatinus, *Z. Kristallogr*. 2014, **229,** 345-352.

25 International Tables for Crystallography, volume A; Kluwer Academic Publishers, Dordrecht/Boston/London 1995.

26 L. Néel, *Compd. Rend.,* 1936, **203,** 304-306.

27 L. Néel, *Ann. Phys. (Paris),* 1948, **3,** 137-198.

28 J. S. Smart, *Am. J. Phys.* 1955, **23,** 356-370.

29 M. Mączka, A. Pietraszko, A. Pikul, K. Hermanowicz, *J. Solid State Chem*. 2016, **233,** 455-462.

30 (a) Z. Wang, X. Zhang, S. R. Batten, M. Kurmoo, S. Gao, *Inorg. Chem.,* 2007, **46,** 8439-8441; (b) M.-Y. Li, M. Kurmoo, Z.-M. Wang, S. Gao, *Chem. Asian J.*, 2011, **6,** 3084-3096.

31 R. Shang, S. Chen, K.-L. Hu, Z.-C. Jiang, B.-W. Wang, M. Kurmoo, Z.-M. Wang, S. Gao, *APL Mater*. 2014, **2,** 124104.

32 R. Shang, G.-C. Xu, Z.-M. Wang, S. Gao, *Chem. Eur. J*. 2014, **20,** 1146-1158.

33 A. Molak, M. Paluch, S. Pawlus, J. Klimontko, Z. Ujma, I. Gruszka, *J. Phys. D: Appl. Phys.* 2005, **38,** 1450-1460.

34 B. Pato Dolán, M. Sánchez-Andújar, L. C. Gómez-Aguirre, S. Yáñez-Vilar, J. Lopez-Beceiro, C. Gracia-Fernandez, A. A. Haghighirad, F. Ritter, S. Castro-Garcia and M. A. Señaris-Rodriguez, *Phys. Chem. Chem. Phys*., 2012, **14**, 8498-8501.

35 (a) M. Mączka, M. Ptak and L. Macalik, *Vib. Spectrosc*., 2014, **71**, 98-104. (b) M. Mączka, W. Zierkiewicz, D. Michalska and J. Hanuza, *Spectrochim. Acta A*., 2014, **128**, 674-680. (c) M.Maczka, K. Szymborska-Małek, A. Ciupa, J. Hanuza, J. *Vib. Spectrosc.* 2015, *77***,** 17-24.

36 D. Zeroka, J. O. Jensen, A. C. Samuels, *J. Mol. Struct*. 1999, **465,** 119-139.

37 A. Ouasri, A. Rhandour, M.-C. Dhamelincourt, P. Dhamelincourt, A. Mazzah, *Spectrochim. Acta A* 2003, **59,** 357-362.

38 P. S. R. Prasad, *J. Phys. Chem*. 1996, **100,** 888-890.

39 A. F. Jalbout, A. Ouasri, H. Jeghnou, A. Rhandour, A. *Vib. Spectrosc.* 2007, **44,** 94-100.

Mixed-valence iron(II)-iron(III) formate framework templated by diethylammonium cations exhibits structural and magnetic phase transitions near 240 and 39 K, respectively

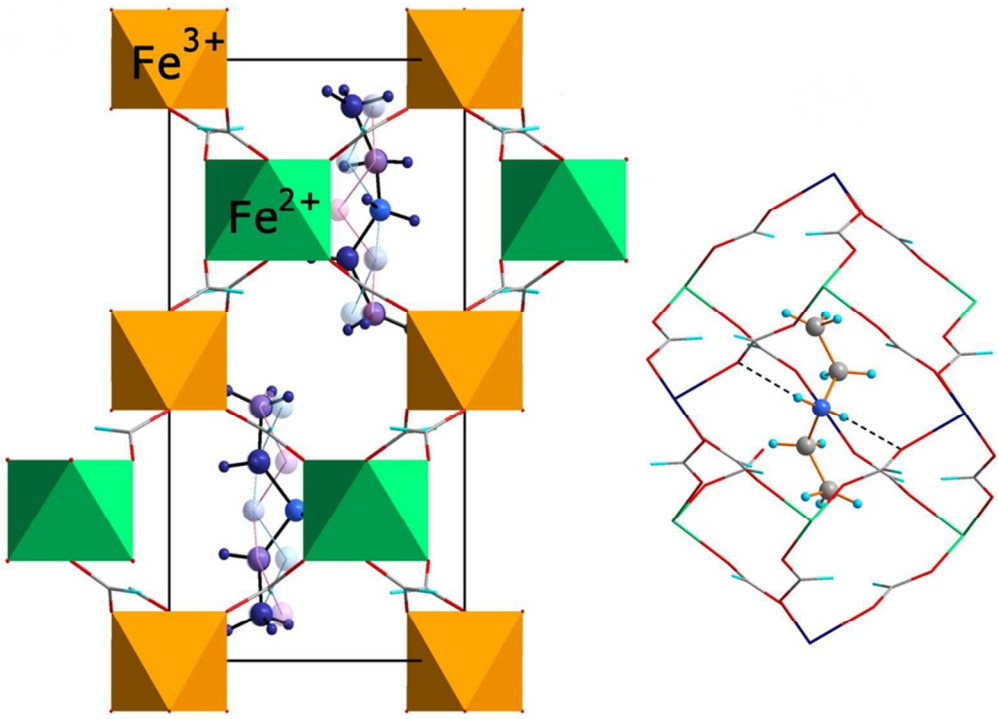

39x28mm (600 x 600 DPI)